Materials Science and Engineering C 45 (2014) 306–312

Contents lists available at ScienceDirect

Materials Science and Engineering C

journal homepage: www.elsevier.com/locate/msec

Preparation, characterization and in vitro gentamicin release of porous HA microspheres

Min Yu, Kechao Zhou, Zhiyou Li, Dou Zhang *

State Key Laboratory of Powder Metallurgy, Central South University, Changsha, Hunan 410083, PR China

ARTICLE INFO

Article history:
Received 15 March 2014
Received in revised form 15 July 2014
Accepted 31 August 2014
Available online 16 September 2014

Keywords:
Hydroxyapatite
Pore structures
Porosities
Drug release

ABSTRACT

Hydroxyapatite (HA) microspheres with high porosities were successfully obtained using an improved ice-templated spray drying (ITSD) technique for drug delivery applications. Pore structures and pore sizes of microspheres have great impact on drug loading and release kinetics. Therefore, solvent types, polyvinyl alcohol (PVA) contents and solid loadings of suspensions were adjusted to control the pore structures and pore sizes. Microspheres with interconnected pore networks and aligned pore structures were obtained using camphene-based and tert-butyl alcohol (TBA)-based suspensions, respectively. With the increase of PVA contents in suspensions, the growth of sintering neck became more obvious and the surface of HA particles became smoother. The inner pore structures of microspheres transformed from uniformly distributed cellular pores to three-dimensional interconnected pore networks, with the increase of solid loadings in suspensions. Gentamicin was successfully loaded into porous HA microspheres. The drug loading percentage increased from 40.59 to 49.82% with the increase of porosity of HA microspheres. The release percentage during the initial 18 h increased from 48.72 to 65.68% with the transformation of pore structures from independent cellular pores (main diameter ~ 3 μm) to three-dimensional interconnected pore networks (main diameter > 3 μm).

1. Introduction

Particulate systems for drug delivery have gained much attention in both research and industry, due to their predictable therapeutic response, prolonged drug release time and great efficacy [1–4]. Irregularly or densely packed particles often cause inflammatory reactions and impede the bone formation, while uniformly packed spherical particles contribute to bone in-growth and avoid inflammation [5]. Porous spherical particles have been generally utilized as fillers or packing materials in orthopedic and maxillofacial applications [6]. For nanospheres, their nano-sized dimension has restricted their application in cell-based therapy for bone-tissue engineering [7]. In contrary, porous microspheres can be well utilized for the delivery of macromolecules, drugs or cells, due to their micro-sized dimension, macro-pores and unique packing properties [8]. Packed microspheres form a matrix with uniform pores between particles, leading to efficient conduction of bone among particles [9]. For drug delivery systems, the pore structure and pore size of microspheres significantly influenced the drug release behavior [10]. The initial release rate depended much on the relation between hydrodynamic diameters and pore sizes of microspheres while the long-term release rate was predominantly controlled by the network of much smaller meshes [11]. Therefore, the pore structure and pore size are two key parameters for modulating drug loading and release behaviors.

Various methods have been applied for fabricating porous microspheres, including freeze-photocuring-casting (FPC) [12], thermal decomposition [13] and spray drying [14]. However, those methods generally have narrow application fields or show poor controllability of pore sizes and pore structures. Spray drying technique has a wide industrial application owing to its simple procedure. Ice-templating method has been widely utilized to fabricate porous materials with generally aligned pore structures and adjustable pore sizes [15,16]. In our previous work, a novel ice-templated spray drying (ITSD) method was developed to fabricate porous microspheres with controlled pore structures and pore sizes, taking advantages of ice-templating method and spray drying technique [17]. Compared to the spray freeze drying technique for producing irregular particles with low porosities [18,19], the improved ITSD technique provides a controllable temperature gradient to fabricate microspheres with adjustable pore structures and high porosities.

Bioceramics have been applied clinically as bone implants, including hydroxyapatite (HA) [20,21], tricalcium phosphate (TCP) [22] and bioglass [23]. Calcium phosphates have been considered as a potential material for drug delivery systems, due to its ability to release a therapeutic agent in situ for producing osteoconductivity of the material [24,25]. As the major component of skeletal tissues, hydroxyapatite (HA) has been applied clinically and experimentally in medical and

* Corresponding author. Fax: +86 731 88877196.
E-mail address: dzhang@csu.edu.cn (D. Zhang).

http://dx.doi.org/10.1016/j.msec.2014.08.075
0928-4931/

bioengineering fields owing to its excellent biocompatibility, biodegradability and osteophony properties [26,27]. As a regular antibiotic, gentamicin can solve bone infection problems caused by the poor circulation of blood in osseous tissues to reach an adequate therapeutic level in the affected regions [28].

In this study, HA microspheres with controlled pore structures and pore sizes were obtained using an improved ITSD technique. Effects of solvent types, PVA contents and solid loadings of the suspensions on pore structures and particle size distributions of HA microspheres were investigated. The relationship between porosities and drug loadings of HA microspheres was investigated. Effects of pore structures and pore sizes of HA microspheres on in vitro release of gentamicin were presented and discussed.

2. Materials and methods

2.1. Fabrication of porous HA microspheres

Hydroxyapatite suspensions were prepared by adding hydroxyapatite powders with a mean particle size of 300 nm (Yipurui Co. Ltd., China) in the solvent of deionized water, camphene (Cuiechem Co. Ltd, China) or tert-butyl alcohol (TBA, Energy Chemical Co. Ltd, China). Ammonium polyacrylate (HydroDisper A160, Otise Co. Ltd, China) and polyvinyl alcohol (PVA, Kuraray Co. Ltd. Japan) were used as the dispersant and binder, respectively. Table 1 lists suspensions with different solvent types, solid loadings, and PVA contents. All suspensions were followed by ball milling for 48 h. Fig. 1 shows the schematic representation of the ITSD process for fabricating porous HA microspheres. Suspensions were sprayed directly into the small cylinder through a circular nozzle (Φ 0.3 mm). The cryogenic atmosphere in the small cylinder was provided by liquid nitrogen between the two steel cylinders, as shown in Fig. 1. The diameters of two cylinders were 12 mm and 8 mm, respectively. The liquid nitrogen volume and spray height were 25 120 mL and 840 mm, respectively. The frozen microspheres were collected and the ice in HA microspheres was subsequently removed in a freeze-drier device (FD-1A-50, Beijing Boyikang Medical Equipment Co. Ltd, China) at −60 °C. The dried HA microspheres were heated up to 600 °C at a heating rate of 1 °C/min and sintered at 1250 °C for 2 h.

2.2. Encapsulation of gentamicin sulfate (GS) in porous HA microspheres

Porous HA microspheres obtained from suspensions with different solid loadings were applied in the process of gentamicin encapsulation. For each batch, 0.2 g of porous HA microspheres was completely immersed in 6 mL of gentamicin sulfate solution (40 IU/mL) under vacuum at room temperature for 56 h and then dried at room temperature for 24 h.

Percentages of GS loadings were estimated through an indirect method, by calculating the difference of GS concentrations in the loading buffer solution, before and after loading. Percentage of drug loading was calculated using the formula [9]:

$$\text{Percentage drug loading} = \frac{X-Y}{X} \times 100\%$$

where X and Y represent the initial and final GS concentrations, respectively. Each test was performed in triplicate.

Table 1
A list of suspension compositions.

Suspension series	Solvent type	Solid loading[a]	PVA content[b]	Ammonium polyacrylate content[b]
I	Camphene	25.9	0	1.0
II	TBA	25.9	0	1.0
III	Water	25.9	0.5	1.0
IV	Water	25.9	1.0	1.0
V	Water	25.9	1.5	1.0
VI	Water	25.9	0	1.0
VII	Water	13.1	0	1.0
VII	Water	7.8	0	1.0

[a] wt.% in relation to the total amount of suspensions.
[b] wt.% in relation to the amount of HA powders.

2.3. In vitro release of gentamicin from GS-loaded HA microspheres

The in-vitro release of gentamicin from GS-loaded HA microspheres was performed in phosphate buffer saline (PBS, pH 7.4) at 37 °C. For each batch, 100 mg of GS-loaded HA microspheres was completely immersed in 10 mL of PBS solution. 3 mL of the release medium was collected at predetermined time intervals and then replaced by a fresh PBS solution (3 mL) each time. The collected release medium was measured at λ = 248 nm using a UV spectrophotometer (UV-6100S, METASH, China). Each test was performed in triplicate.

2.4. Characterization

The morphologies of HA microspheres were measured using a scanning electron microscope (SEM, Nova NanoSEM 230, USA) at an acceleration voltage of 10 kV and a distance of 7 mm. Each sample was coated with gold prior to imaging. The particle size distributions of HA microspheres were measured using a laser diffraction scattering particle sizer (Malvern Mastersizer, USA). The presence of carbon in GS-loaded HA microspheres was verified using the Energy Dispersive X-ray Spectrometer (EDS, Norman Instrument, USA) at an acceleration voltage of 20 kV and a distance of 7 mm. The pore size distributions of porous HA microspheres were measured using the mercury intrusion porosimetry (AutoPore IV 9500, Micromeritics, USA). The Hg-surface tension at 20 °C corresponds to 485 dyn/cm. The contact angle and the density of Hg were 130° and 13.5 g/cm^3, respectively. The pore diameter was calculated according to the Wasburn equation [29,30]:

$$D = \frac{-4\gamma\cos\theta}{P}$$

where D is the pore diameter (μm); γ is the surface tension of mercury (dynes/cm); θ and P are the contact angle (°) and the pressure (psia).

The element contents of carbon and nitrogen in GS-loaded HA microspheres were measured using the CS-444 infrared carbon–sulfur analyzer (LECO, USA) and the TC-436 oxygen–nitrogen analyzer (LECO, USA), respectively. The porosities of porous HA microspheres were measured based on Archimedes' principle. 1 g of dried HA microspheres for each sample was used to measure the porosity. The porosity (P) was calculated according to the following formula:

$$P = \frac{W_2 - W_1}{W_2 - W_1 + \rho_0 V_0} \times 100\%$$

where W_1 is the weight of sample in air, W_2 is the weight of sample with water, ρ_0 is the density of water (1.0 g/mL), V_0 is the increased volume of water caused by the immersed HA microspheres in water. In order to ensure the accuracy of W_1, HA microspheres were dried for 5 h in the vacuum drying chamber (P2F-6050, Jinghong Co. Ltd., China). The dried sample was immersed in water and then the increased volume of water was measured as V_0. Each test was performed in triplicate.

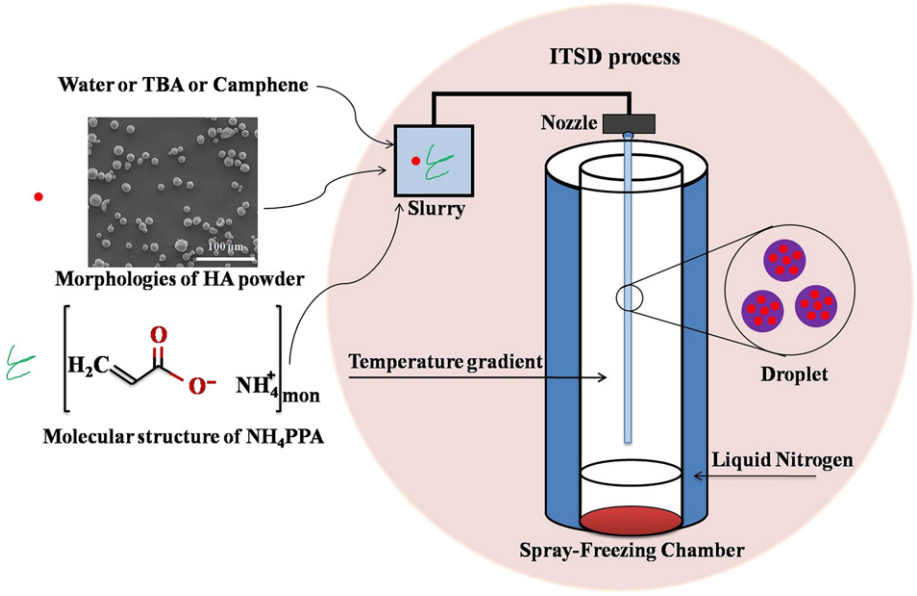

Fig. 1. Schematic representation of the ITSD process for porous HA microspheres.

3. Results and discussions

3.1. Microstructure characterization

3.1.1. Effect of solvents

Fig. 2 shows the surface and internal morphologies of sintered HA microspheres obtained from suspensions with 25.9 wt.% solid loading, based on camphene and TBA solvents. As shown in Fig. 2a and c, dendritic and interconnected pore structures in the HA microspheres were obtained from camphene-based suspensions after removing the frozen camphene. The HA microspheres obtained from TBA-based suspensions showed the long-range aligned pores on the surface of microspheres (Fig. 2b) and short-range aligned inner pores (Fig. 2d). As shown in Fig. 2a and c, the pore size of inner pores (>3 μm) was much larger than that of surface pores (<1 μm). Fig. 2d shows the mean thickness of aligned pores was about 2 μm. These can be explained by the mechanism of crystal growth in the liquid droplets during the freezing process. The camphene crystals grew dendritically in certain crystallographic directions, resulting in dendritic and interconnected pore structures [31]. Among three crystalline phases of tert-butyl alcohol (TBA), stable phase II formed unidirectional crystals under directional temperature gradients, resulting in aligned pore channels [32,33]. During the freezing process, the rapid temperature decrease around the surface of liquid droplets contributed to the long-range

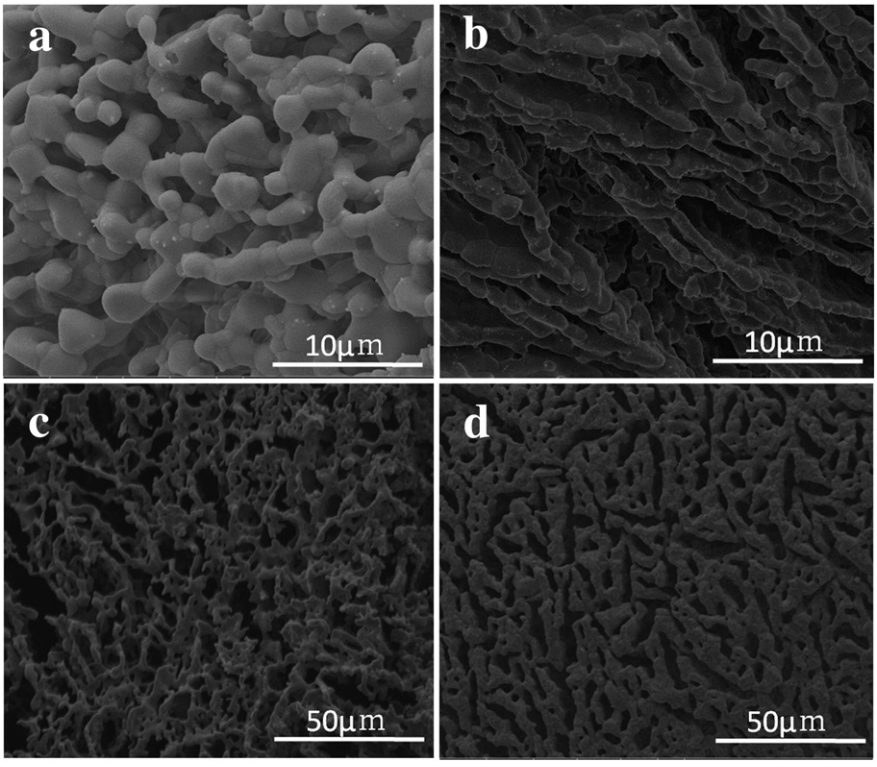

Fig. 2. The surface morphologies (a and b) and cross-sectional views (c and d) of sintered HA microspheres fabricated by suspension I (a and c) and suspension II (b and d).

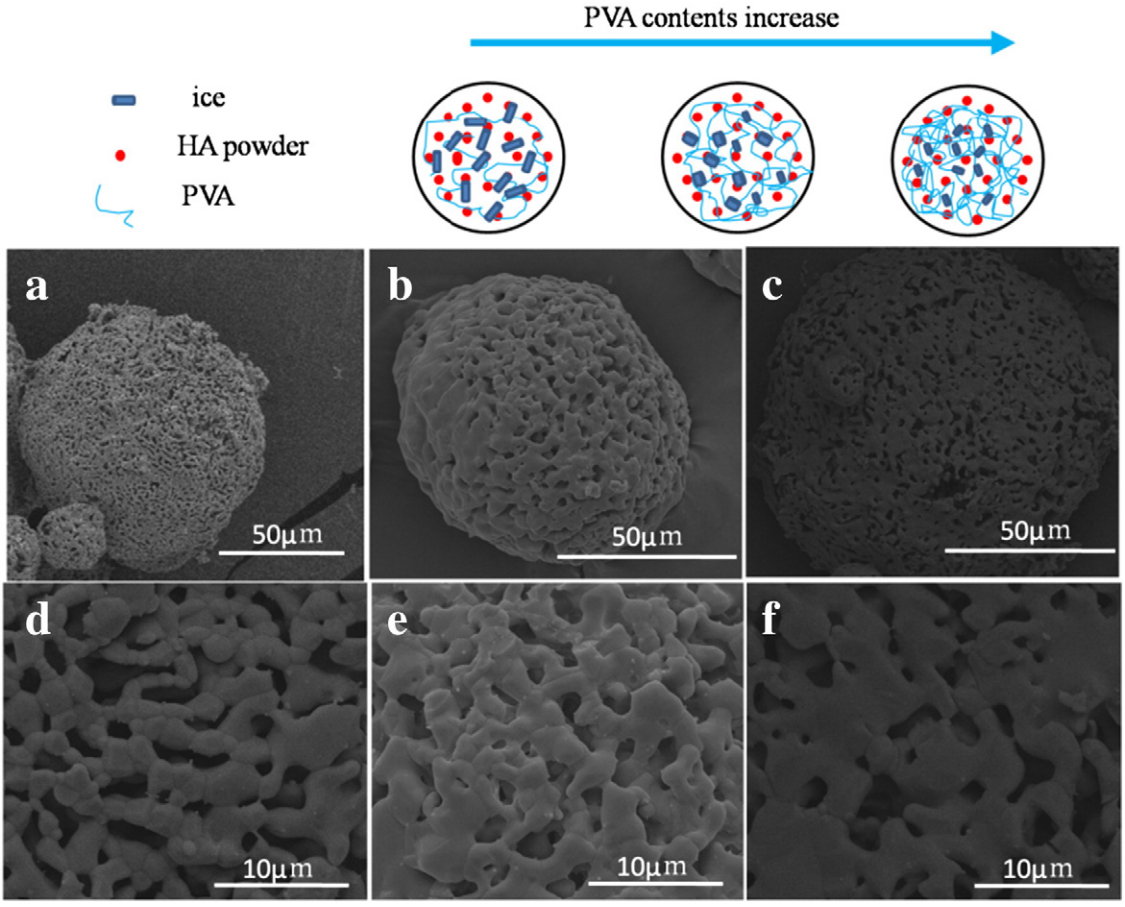

Fig. 3. Surface morphologies of sintered HA microspheres fabricated from suspensions with different PVA contents: (a) suspension III, (b) suspension IV, and (c) suspension V. (d), (e) and (f) are the surface morphologies of microspheres in (a), (b) and (c) at higher magnification, respectively.

aligned pore structures while the relatively slow temperature decrease inside liquid droplets led to the short-range aligned pores [32].

3.1.2. Effect of PVA contents

Fig. 3a, b and c shows the surface morphologies of sintered HA microspheres obtained from water-based suspensions with different PVA contents of 0.5 wt.%, 1.0 wt.% and 1.5 wt.%, respectively. Sintered HA microspheres in this study can fulfill the required mechanical properties for their functions without introducing any non-degradable or poor-biocompatible ingredients. All porous HA microspheres showed a high sphericity degree. As shown in Fig. 3d, HA microspheres obtained from suspensions with 0.5 wt.% PVA content showed the largest mean pore size (about 1 μm) and the mixture of short-range aligned pores and cellular pores. As shown in Fig. 3e and f, HA microspheres obtained from suspensions with 1.0 wt.% and 1.5 wt.% PVA contents showed the interconnected pore structures and the absence of the grain boundaries which appeared clearly in Fig. 3d. The growth of sintering neck and the smooth surface of HA particles became more obvious, with PVA contents increasing from 0.5 to 1.5 wt.%. As the binder encapsulating HA grains, increased PVA contents contributed to reducing the distance between HA grains, promoting intense sintering procedures.

To some extent, the PVA contents also influenced pore structures of HA microspheres fabricated using the ITSD technique. This can be explained by the resistance of ice crystal growth. With the increase of PVA contents in suspensions, PVA easily formed the interconnected membrane which encapsulated HA powders [34]. The relatively low PVA content in suspensions prevented gelled PVA from forming continuum so that ice crystals easily grew directly, resulting in long-range aligned pores after sublimation. The increased PVA content formed interconnected flaky shape gels which obstructed the direct growth of ice crystals during the freezing process, resulting in short-range aligned pores. The high PVA content contributed to interconnected and immovable networks which significantly obstructed the direct growth of ice crystals during the freezing process, leading to the disappearance of aligned pores and the appearance of interconnected pore structures after sublimation.

3.1.3. Effect of solid loadings

Fig. 4 shows cross-sectional morphologies of sintered HA microspheres fabricated from water-based suspensions with different solid loadings of 25.9 wt.%, 13.1 wt.% and 7.8 wt.%. The inner pore structures of HA microspheres transformed from the uniformly distributed cellular pores (Fig. 4a) to the three-dimensional interconnected networks (Fig. 4c), with solid loadings increasing from 7.8 to 25.9 wt.%. As shown in Fig. 4b, HA microspheres obtained from suspensions with 13.1 wt.% solid loading showed the combination of interconnected pore networks (pore size: 2.5–5 μm) with small cellular pores (pore size < 2.5 μm). As shown in Fig. 4e, f and g, the sintering neck growth became more obvious and the surface of particles became smoother, with solid loadings increasing from 7.8 to 25.9 wt.%. Suspensions with low solid loadings contributed to more tiny pores between HA particles, leading to obstructing the intense sintering. For drug delivery systems, particles with smoother surfaces are generally required due to their ability to induce a less inflammatory reaction and significantly faster ingrowth of bone than rougher materials [35].

Fig. 5a shows the particle size distributions of porous HA microspheres obtained from water-based suspensions with different solid loadings. Porous HA microspheres obtained from 13.1 wt.% and 7.8 wt.% suspensions displayed relatively narrower particle size distributions and smaller mean particle sizes than those from 25.9 wt.%

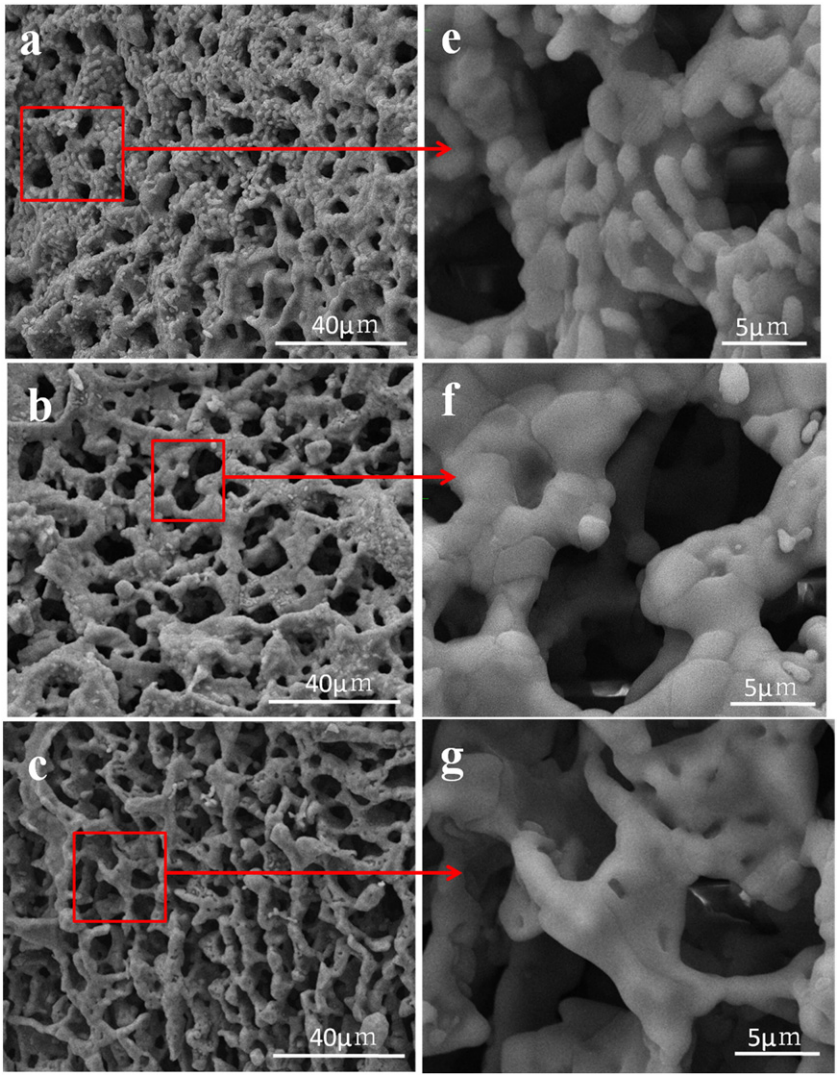

Fig. 4. Cross-sectional views of sintered HA microspheres fabricated from suspensions with different solid loadings: (a) suspension VI, (b) suspension VII, and (c) suspension VII.

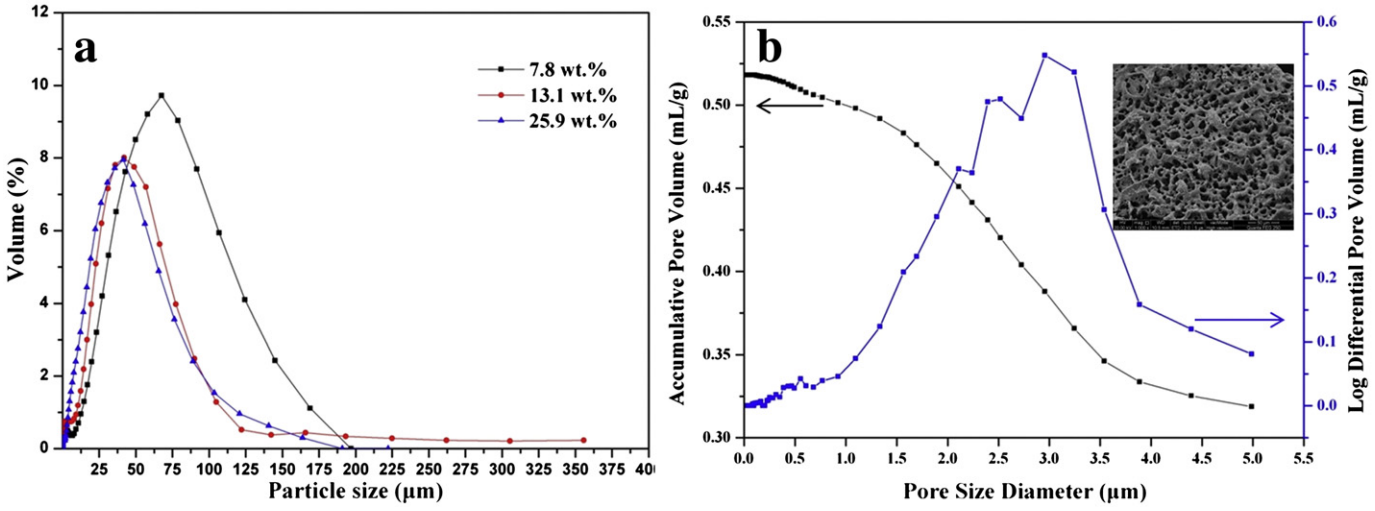

Fig. 5. The particle size distributions (a) of porous HA microspheres fabricated from suspensions VI, VII and VII, and pore size distribution (b) of porous HA microspheres fabricated from suspension VII.

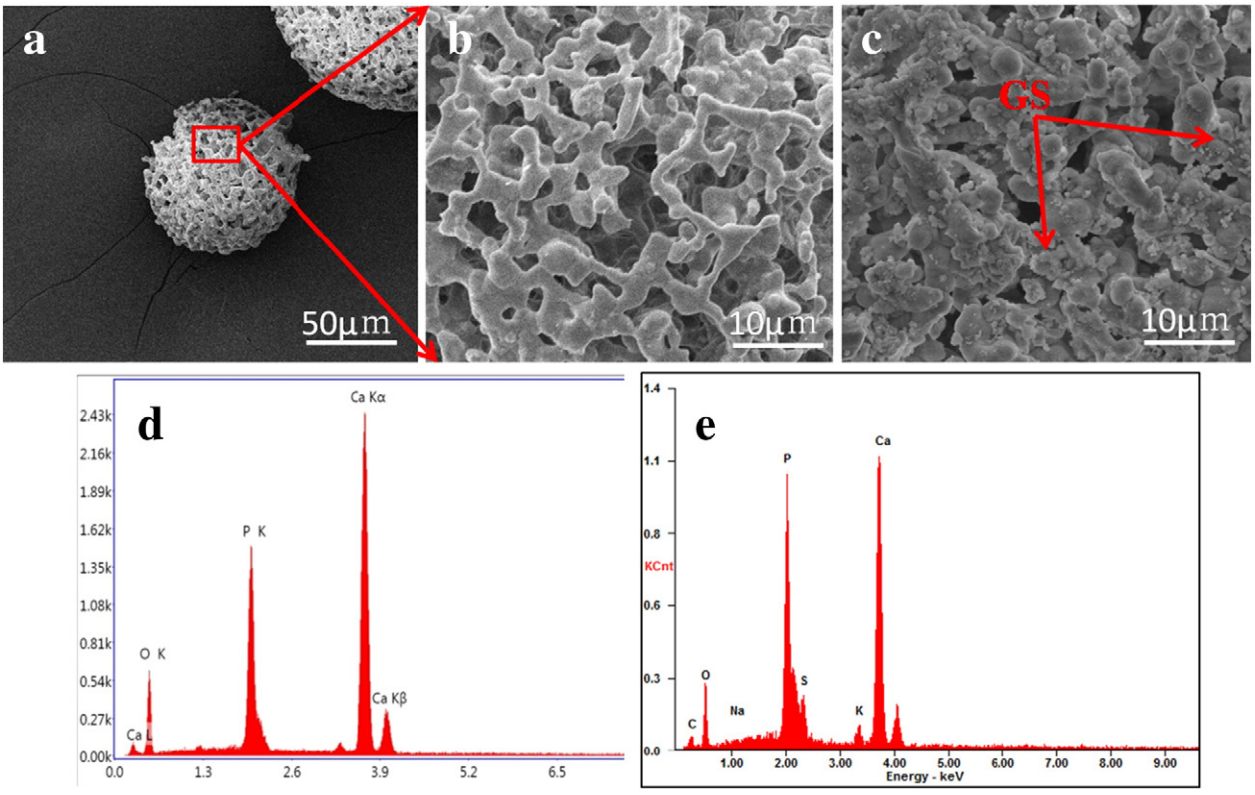

Fig. 6. The surface morphologies and EDS patterns of sintered HA microspheres (a, b and d) and GS-loaded HA microspheres (c and e).

suspensions. The mean particle sizes of HA microspheres were about 80 μm, 50 μm and 50 μm for solid loadings of 25.9 wt.%, 13.1 wt.% and 7.8 wt.%, respectively. Fig. 5b shows the pore size distribution of porous HA microspheres obtained from water-based suspensions with 13.1 wt.% solid loading. The pore sizes mainly distributed in the range of 0.5–5 μm and the main pore size was about 3 μm, which was in good agreement with the SEM micrograph in Fig. 3c. Suspensions with low solid loadings were more likely to form smaller HA liquid droplets during the spray process, leading to smaller mean particle sizes after sintering.

3.2. Effect of pore structures on the encapsulation and release of gentamicin

Fig. 6 shows the surface morphologies and EDS patterns of sintered HA microspheres and GS-loaded HA microspheres. As shown in Fig. 6a and b, HA microspheres exhibited a well-defined spherical shape and open and interconnected pore networks with the mean pore size of about 3 μm. When comparing morphologies of HA microspheres before (Fig. 6b) and after (Fig. 6c) drug loading, it can be concluded that gentamicin was successfully loaded into porous HA microspheres and distributed on both outer surface and inner part of HA microspheres. As shown in Fig. 6d and e, the sintered HA microspheres showed the absences of C and S elements, while the GS-loaded HA microspheres showed the presences of C and S elements, which were only possessed by GS ($C_{21}H_{45}N_5O_{11}S$). The presence of K and Na elements in the GS-loaded microspheres resulted from PBS solution which contained K and Na ions.

The element contents of N, C, O, H and S in GS-loaded HA microspheres were measured using infrared carbon–sulfur analyzer and oxygen–nitrogen analyzer. As shown in Table 2, the content of O was the highest among the element contents of N, C, O, H and S, due to the presences of both HA ($Ca_{10}(PO_4)_6(OH)_2$) and GS ($C_{21}H_{45}N_5O_{11}S$). The contents of N, C and S were 2.43%, 4.92%, and 0.63%, respectively, owing to the presence of GS. The elemental mass ratio of N/C/S in GS-loaded HA microspheres was 1:2.1:0.259, in agreement with the N/C/S atomic mass ratio (1:3.5:0.457) in GS ($C_{21}H_{45}N_5O_{11}S$).

Table 2
Element contents in the GS-loaded HA microspheres.

Element	N	C	O	S	H
Content (wt.%)	2.43	4.92	30.28	0.63	1.57

The relationship between porosities and drug loadings of HA microspheres was investigated in this work. The percentages of GS loadings in HA microspheres were measured using the formula given in the experimental section. As shown in Fig. 7, both the porosities and drug loadings of HA microspheres decreased, with solid loadings of suspensions increasing from 7.8 to 25.9 wt.%. The percentages of GS loadings in microspheres decreased from 49.8 to 40.6%, with porosities of microspheres decreasing from 81.3 to 63.2%. It is well known that porosities greatly influenced the drug loading kinetic [36]. These can

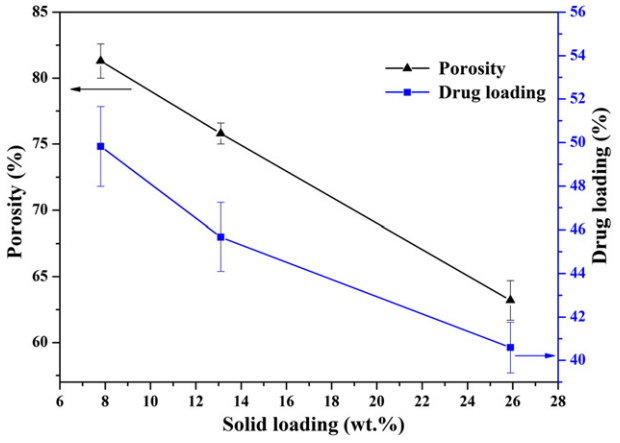

Fig. 7. Porosities and drug loadings of HA microspheres versus solid loadings of suspensions.

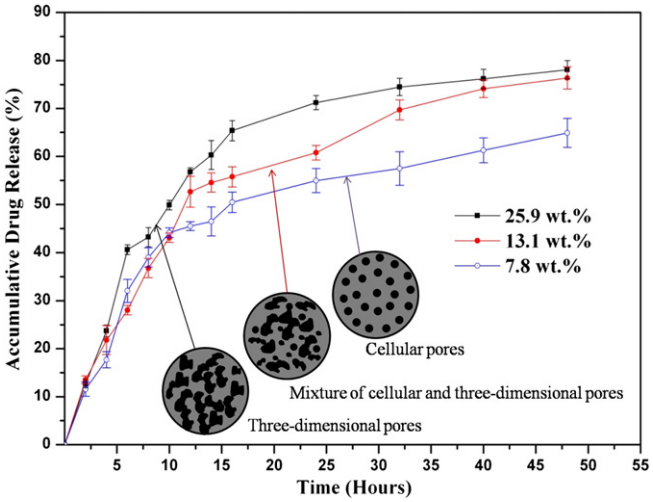

Fig. 8. The in vitro releases of gentamicin from GS-loaded HA microspheres fabricated from suspensions with different solid loadings.

be explained by the amount of ice crystals in the frozen microspheres and free space in sintered microspheres. Suspensions with lower solid loadings formed more ice crystals as template, resulting in higher porosities of microspheres. Higher porosities provided more free space for gentamicin to deposit on HA microspheres, leading to higher drug loadings. Compared to bioactive ceramic microspheres obtained using other methods [7,37], porous HA microspheres fabricated using the ITSD technique showed much higher porosities which are conducive to higher drug loadings.

Fig. 8 shows the in vitro releases of gentamicin from GS-loaded HA microspheres obtained from suspensions with different solid loadings. All HA microspheres showed a high gentamicin release rate for the initial 16 h, a relatively lower rate for the following 20 h and a very low rate after 36 h. During the initial 18 h, about 65%, 55% and 48% of the loaded-GS amount were released from HA microspheres obtained from 25.9 wt.%, 13.1 wt.%, and 7.8 wt.% suspensions, respectively. Between 16 h and 48 h, less than 15% of loaded-GS amount was released from all three kinds of GS-loaded HA microspheres. It is well known that pore sizes of microspheres greatly influenced the drug release kinetics [11]. The initial burst release rate mainly depended on open and connected macropores, while the slow release rate in the last period was mainly controlled by the small pores. During the initial 18 h, the three-dimensional and interconnected pore networks (pore size > 3 μm, Fig. 4a) resulted in the highest gentamicin release percentage (~65%), while the independent cellular pores (pore size ~ 3 μm, Fig. 4c) contributed to the lowest release percentage (~48%). Therefore, pore structures of microspheres also greatly influenced the gentamicin release kinetics.

4. Conclusions

An improved ice-template spray drying technique was proposed to produce porous HA microspheres with controlled pore structures and the mean particle sizes of 50–85 μm. Solvent types, PVA contents and solid loadings of suspensions were adjusted to control pore structures of HA microspheres. Camphene-based and TBA-based suspensions were utilized to fabricate coarse interconnected pore structures and aligned pore structures with long-range surface pores and uniform short-range inner pores, respectively. The growth of sintering neck became more obvious and the surface of HA particles became smoother, with PVA contents increasing from 0.5 to 1.5 wt.%. The inner pore structures transformed from uniformly distributed cellular pores to three-dimensional and interconnected pore networks, with solid loadings increasing from 7.8 to 25.9 wt.%. Gentamicin was successfully loaded into porous HA microspheres. The drug loading percentages increased from 40.59 to 49.82%, with porosities of microspheres increasing from 63.2 to 81.3%. The release amount percentage during the 18 h period increased from 48 to 65%, when pore structures transformed from the independent cellular pores (pore size ~ 3 μm) to the three-dimensional and interconnected pore networks (pore size > 3 μm). All HA microspheres showed an initial high gentamicin release rate for the initial 16 h, a relatively lower rate for the following 20 h and a very low rate after 36 h.

Acknowledgments

The authors are grateful to the National Natural Science Foundation of China (No. 51172288), the Ph.D. Programs Foundation of Ministry of Education of the People's Republic of China (Nos. 20110162130003 and 20110162110044), and the Graduate Innovation Program Foundation of Central South University (No. 72150050547) for the financial support.

References

[1] J.W. Yoo, D.J. Irvine, D.E. Discher, S. Mitragotri, Nat. Rev. Drug Discov. 10 (2011) 7.
[2] A.J. O'Connor, F. Caruso, Nature 502 (2013) 7471.
[3] E. Mathiowitz, J.S. Jacob, Y.S. Jong, G.P. Carino, Nature 386 (1997) 6623.
[4] S. Parveen, R. Misra, S.K. Sahoo, Nanomed. Nanotechnol. Biol. Med. 8 (2012) 2.
[5] B.S. Chang, K.S. Hong, H.J. Youn, H.S. Ryu, Biomaterials 21 (2000) 12.
[6] D. Arcos, R.M. Vallet, Acta Mater. 61 (2013) 3.
[7] C. Wu, H. Zreiqat, Acta Biomater. 6 (2010) 3.
[8] J. Fang, Y. Zhang, S. Yan, Z. Liu, Acta Biomater. 10 (2014) 1.
[9] M. Sivakumar, R.K. Panduranga, Biomaterials 23 (2002) 15.
[10] S. Schacht, Q. Huo, M.I. Voigt, G. Stucky, 273 (1996) 768.
[11] A. Bertz, B.S. Wöhl, S. Miethe, B. Tiersch, J. Biotechnol. 163 (2012) 243.
[12] Y. Hazan, J. Am. Ceram. Soc. 1 (2012) 95.
[13] G. Sharma, J. Pethaiyan, Cambridge Univ. Press 13 (2013) 1547.
[14] K. Möbus, J. Siepmann, R. Bodmeier, Eur. J. Pharm. Biopharm. 1 (2012) 81.
[15] K.C. Zhou, Y. Zhang, D. Zhang, X. Zhang, Scr. Mater. 5 (2011) 64.
[16] K. Moebus, J. Siepmann, R. Bodmeier, J. Control. Release 2 (2012) 157.
[17] M. Yu, K. Zhou, Y. Zhang, D. Zhang, Ceram. Int. 40 (2014) 1215.
[18] H.R. Costantino, L. Firouzabadian, C. Wu, et al., J. Pharm. Sci. 2 (2002) 91.
[19] Y.F. Maa, P.A. Nguyen, T. Sweeney, Pharm. Res. 2 (1999) 16.
[20] G.A. Gholami, B. Najafi, F. Mashhadiabbas, W. Goetz, Clin. Oral Implants Res. 10 (2012) 23.
[21] D. Dallari, L. Savarino, U. Albisinni, P. Fornasari, Biomaterials 1 (2012) 33.
[22] J.S. Lee, U.M. Wikesjö, U.W. Jung, S.H. Choi, J. Clin. Periodontol. 4 (2010) 37.
[23] L. Xia, D. Zeng, X. Sun, Y. Xu, et al., Microporous Mesoporous Mater. 3 (2013) 173.
[24] J. Guicheux, G. Grimandi, M. Trécant, A. Faivre, J. Biomed. Mater. Res. 2 (1997) 34.
[25] C. Ragel, R.M. Vallet, J. Biomed. Mater. Res. 3 (2000) 51.
[26] C. Yang, Y. Liu, Y. He, Y. Du, Biomaterials 2 (2013) 34.
[27] J.S. Son, M. Appleford, J.L. Ong, J.C. Wenke, J. Control. Release 2 (2011) 153.
[28] C.G. Zalavras, M.J. Patzakis, Surg. Infect. 4 (2012) 6.
[29] M. Virto, P. Frutos, S. Torrado, G. Frutos, Biomaterials 1 (2003) 24.
[30] S. Joschek, B. Nies, R. Krotz, A. Göpferich, Biomaterials 16 (2000) 21.
[31] J. Han, C. Hong, X. Zhang, J. Du, W. Zhang, J. Eur. Ceram. Soc. 1 (2010) 30.
[32] L. Hu, C.A. Wang, Y. Huang, C. Sun, et al., J. Eur. Ceram. Soc. 16 (2010) 30.
[33] R. Chen, C.A. Wang, Y. Huang, L. Ma, et al., J. Am. Ceram. Soc. 11 (2007) 90.
[34] K.H. Zuo, Y.P. Zeng, D. Jiang, Mater. Sci. Eng. C 2 (2010) 30.
[35] A. Figueiredo, P. Coimbra, A. Cabrita, F. Guerra, M. Figueiredo, Mater. Sci. Eng. C 12 (2013) 33.
[36] R. Byrne, P. Deasy, Int. J. Pharm. 1 (2002) 246.
[37] W. Paul, C. Sharma, J. Mater. Sci. Mater. Med. 7 (1999) 10.